# Effect of insertion of ultrathin $Al_2O_3$ interlayer at metal/GaN interfaces

**Masamichi Akazawa [*,1] and Taito Hasezaki[1]**

[1] Research Center for Integrated Quantum Electronics, Hokkaido University, 060-0813, Sapporo, Japan

Received ZZZ, revised ZZZ, accepted ZZZ
Published online ZZZ (Dates will be provided by the publisher.)

**Keywords** GaN, Schottky barrier, $Al_2O_3$, interlayer.

* Corresponding author: e-mail akazawa@rciqe.hokudai.ac.jp, Phone: +81 11 706 6875, Fax: +81 11 716 6004

Fermi level depinning at a metal/semiconductor interface by using an ultrathin insulating interlayer to block the penetration of the metal wave function into the semiconductor was examined on GaN. A Si-doped n-type GaN epitaxial layer on a freestanding GaN substrate was used as the host material. For the samples with an interlayer, an ultrathin $Al_2O_3$ layer of 1 nm thickness was deposited by atomic layer deposition. As the metal layers, Ag, Cu, Au, Ni, and Pt were deposited by electron beam evaporation. Samples without an interlayer were also fabricated for comparison. The apparent change in current-voltage characteristics of the Schottky barrier diodes with the insertion of the interlayer was dependent on the electrode metal. However, the apparent Schottky barrier height (SBH) for the samples with the interlayer was almost constant and independent of the metal electrode, although the samples without an interlayer exhibited a moderate dependence of the SBH on the metal work function. Thus, the pinning became stronger upon the insertion of the interlayer, although blocking of the metal wave function by using an ultrathin insulator was expected to lead to depinning.



**1 Introduction** Metal-semiconductor interfaces are essential building blocks in semiconductor devices. The Schottky barrier height (SBH) is the most important parameter of metal-semiconductor interfaces. Ideally, the SBH can be changed by varying the work function of the metal. However, in most semiconductors, the change in the SBH is severely limited even for a large change in the metal work function [1]. This phenomenon is referred to as Fermi level pinning. Depinning of the Fermi level will increase the flexibility of device design.

Recently, several publications have reported that the insertion of an ultrathin insulating layer led to a modification of the SBH for Si [2-5], Ge [6, 7], GaAs [8], InGaAs [9, 10], and GaN (on sapphire) [11]. The initial explanation for this was that the inserted ultrathin interlayer prevents the generation of metal-induced gap states (MIGS) [12, 13] by blocking the metal wave function acting as a tunnel barrier without disturbing the current flow because of its thinness, resulting in depinning [2, 5, 6]. Actually, the enhancement of the dependence of the SBH on the metal work function by inserting an insulating interlayer has been reported for Si [3, 5] and n-Ge [6]. However, there is also an indication of the work function dependence of the SBH, where the Fermi level is shifted and "pinned" by the insertion of an ultrathin insulating layer, for GaAs [8] and InGaAs [9, 10]. An alternative explanation of this phenomenon that a dipole is generated at the interface has been discussed for Si [4], GaAs [8], and InGaAs [9], while the possibility of pinning at the insulator surface [3] for Si and at the semiconductor surface [9] for InGaAs has been proposed. Therefore, the mechanism is under debate and more data are needed to understand this phenomenon.

III-nitride semiconductors, including GaN as the main material, are attractive materials for optoelectronic [14, 15] and high-power device [16, 17] applications. GaN is a suitable semiconductor for investigating changes in the SBH because of its wide gap, leading to a large change in the current–voltage characteristics if such a change is possible. However, the insertion of an insulating layer at a metal/GaN interface has only been carried out for Fe and Fe/Gd electrodes, without any results for the metal-work-function dependence of the SBH [11], using GaN layers on sapphire substrates. A GaN epitaxial layer on a GaN freestanding substrate is characterized by a low defect density, which leads to excellent rectifying characteristics [18-20]. On the other hand, an $Al_2O_3$/GaN interface formed by

atomic layer deposition (ALD) on such a GaN epitaxial layer has been reported to have a low interface state density [21]. Therefore, inserting an $Al_2O_3$ interlayer at a metal/GaN interface seems to be suitable for the investigation of depinning the Fermi level.

In this study, we investigated the effect of the insertion of an ultrathin $Al_2O_3$ layer at metal/GaN interfaces. Large changes in the apparent SBH were observed for Ag/GaN and Cu/GaN interfaces upon the insertion of an ultrathin $Al_2O_3$ interlayer, while smaller changes were observed for Au, Ni, and Pt electrodes. A change in the metal-work-function dependence of the SBH upon the insertion of the interlayer was observed.

**2 Preparation of samples** Figure 1 illustrates the structure of the sample with an ultrathin $Al_2O_3$ interlayer. The host semiconductor was n-GaN grown by metal-organic vapor phase epitaxy on an $n^+$-GaN (0001) free-standing substrate. The carrier concentration of the 3-μm-thick n-GaN epitaxial layer was adjusted to $5\times10^{16}$ $cm^{-3}$ by Si doping. Prior to the metal and insulator deposition, the GaN surface was treated with a dilute HCl ($HCl:H_2O$ = 1:3) solution for 1 min to remove the surface oxide layer, followed by rinsing in deionized water. As the metal layer, Ag, Cu, Ni, Au, and Pt were deposited by electron beam evaporation. A lift-off technique based on photolithography was used to form a circular electrode. For the sample with the $Al_2O_3$ interlayer, ALD was carried out at a substrate temperature of 300°C using trimethylaluminum (TMA) and water ($H_2O$) precursors. A back ohmic contact was formed by Ti/Au evaporation.

**3 Results and discussion** Figure 2 shows a comparison of the current-density–voltage (*J*–*V*) characteristics of the fabricated diodes (a) with and (b) without the ultrathin $Al_2O_3$ interlayer obtained at room temperature (RT). Excellent rectifying characteristics with the suppression of the leakage current under a reverse bias, owing to the low dislocation density of GaN grown on the GaN freestanding substrate, can be seen. The dependence of the reverse current on the metal was reduced by the insertion of the $Al_2O_3$ interlayer.

The schematic band diagram for the sample with the interlayer is illustrated in Fig. 3. Since the $Al_2O_3$ interlayer is very thin, the electrons can tunnel through the insulator barrier. The effective SBH is defined as the energy difference between the metal Fermi level and the conduction band edge of the semiconductor. The original idea of inserting an ultrathin $Al_2O_3$ interlayer is to suppress the penetration of the metal wave function into the semiconductor for depinning based on the MIGS model. Depinning should result in a situation where the effective SBH is changed in a manner depending on the metal work function, which should result in a large change in *J*–*V* characteristics. However, as can be seen in Fig. 1 (b), the insertion of the interlayer led to a smaller metal-dependent change in *J*–*V* characteristics.

Here the SBH is derived by fitting the forward-bias *J*–*V* characteristics to the thermionic emission (TE) model equation

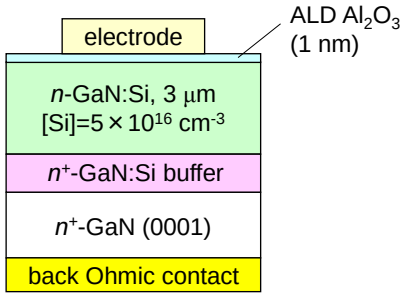


**Figure 1** Structure of sample with $Al_2O_3$ interlayer.

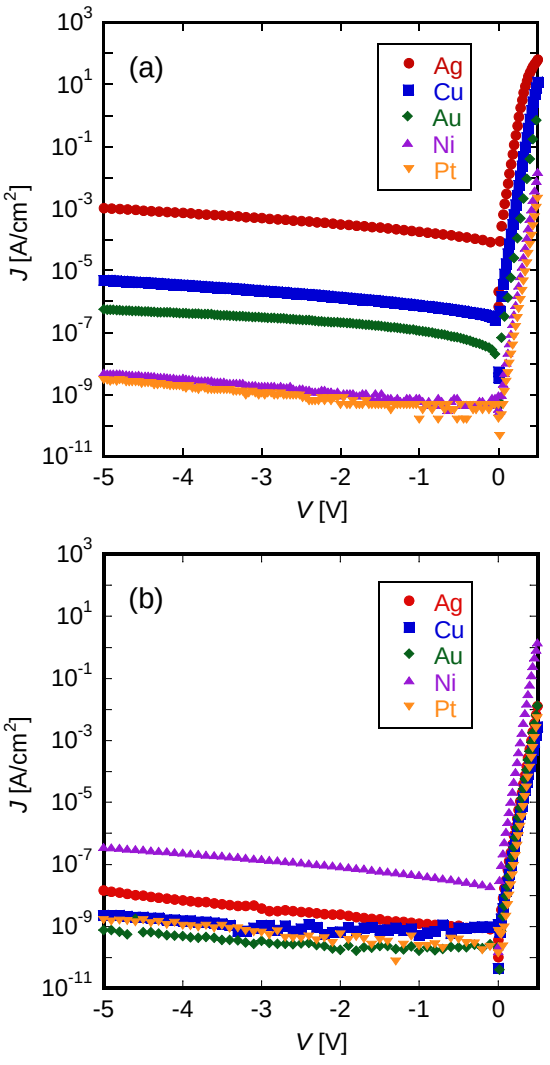

**Figure 2** Summary of measured *J–V* characteristics obtained at RT for samples (a) without and (b) with $Al_2O_3$ interlayer.

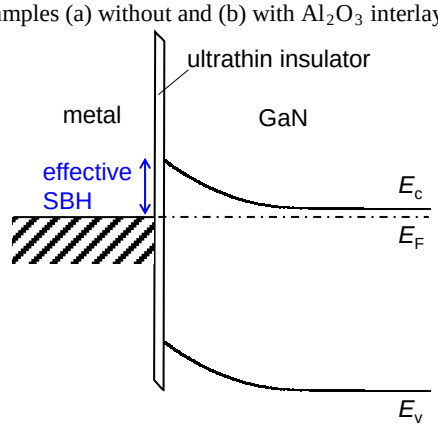


**Figure 3** Schematic band diagram for sample with interlayer.

$$J = A^{*}T^{2}\exp\left(-\frac{q\phi_B}{kT}\right)\exp\left[\left(\frac{qV}{nkT}\right)-1\right]. \qquad (1)$$

Here, $A^*$ is the Richardson constant, $T$ is the temperature, $k$ is the Boltzmann constant, $q$ is the electron charge, $\phi_B$ is the SBH, $n$ is the ideality factor, and $V$ is the forward bias voltage.

For the samples with the interlayer, the following equation introduced in Ref. [1] describes the *J–V* characteristics more precisely:

$$J = A^{*}T^{2}\exp\left(-\frac{2d\sqrt{2qm^{*}\phi_T}}{\mathrm{h}}\right)\exp\left(-\frac{q\phi_{Beff}}{kT}\right) \times\exp\left[\left(\frac{qV}{nkT}\right)-1\right]. \qquad (2)$$

Here $m^*$ is the effective mass of an electron, $\phi_T$ is the tunneling barrier height, $\phi_{Beff}$ is the effective SBH, and h is the reduced Planck constant. In this case, $\phi_{Beff}$ can be extracted from the temperature dependence of the *J–V* characteristics. However, this method cannot be applied to a GaN Schottky barrier diode because the SBH changes with the temperature [20]. Here, we concern ourselves with the effect of interlayer insertion on the *J–V* characteristic as a Schottky barrier diode and its dependence on the electrode metal. Therefore, we use $\phi_B$ derived by Eq. (1) as an apparent SBH in place of $\phi_{Beff}$ for the samples with the interlayer because $\phi_B$ should be changed by an amount depending on the metal electrode if depinning occurs.

Figure 4 shows the forward-bias *J–V* characteristics of the Ag-electrode samples with and without the ultrathin $Al_2O_3$ interlayer at RT. It can be seen that the insertion of the ultrathin $Al_2O_3$ interlayer led to a reduction of the current density by five orders. The linearity of the log *J–V* plots at a low bias is excellent, as fitted by the straight line calculated by Eq. (1). From this fitting, $\phi_B$ was derived to be 0.64 eV for the sample without the interlayer and 0.91 eV for the sample with the interlayer. Therefore $\phi_B$ was increased by 270 meV upon the insertion of the $Al_2O_3$ interlayer. The ideality factors were 1.20 and 1.07 for the samples with and without the interlayer, respectively.

For the Cu electrode, the forward-bias *J–V* characteristics at RT are compared in Fig. 5. Excellent linearity of the log *J–V* plots was again obtained for both samples with and without the interlayer, and a decrease in the current density of at least three orders of magnitude was observed. $\phi_B$ was derived to be 0.75 eV for the sample without the interlayer

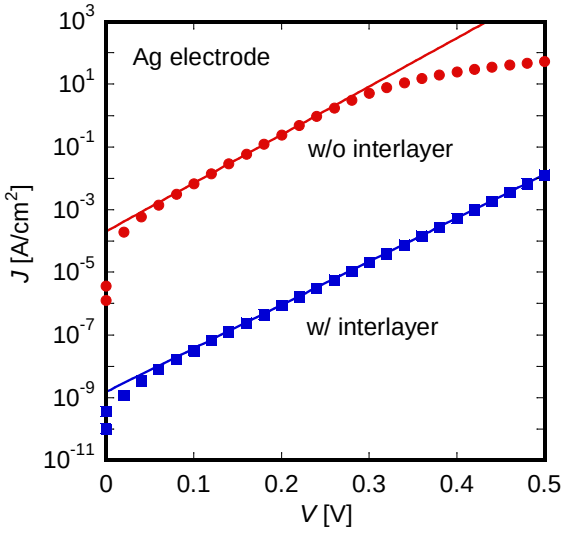


**Figure 4** *J–V* characteristics of the Ag-electrode samples at RT.

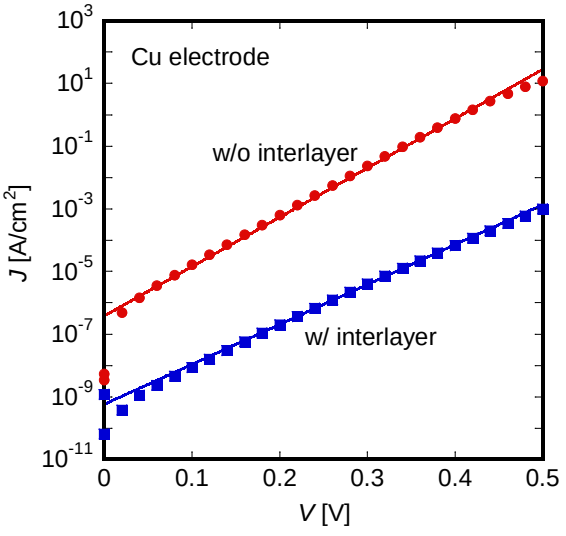

**Figure 5** *J–V* characteristics of the Cu-electrode samples at RT.

and 0.91 eV for the sample with the interlayer. The change in $\phi_B$ with the insertion of the interlayer was 160 meV, smaller than that for the Ag electrode. The ideality factors were 1.27 and 1.07 for the samples with and without the interlayer, respectively.

For the Au electrode, the *J–V* characteristics at RT are plotted in Fig. 6, where a change in the current density of one order of magnitude is indicated along with excellent linearity of the log *J–V* plots. $\phi_B$ was changed from 0.85 eV to 0.94 eV by the insertion of the $Al_2O_3$ interlayer, which corresponds to a change of 90 meV. The ideality factors were 1.07 and 1.05 for the samples with and without the interlayer, respectively.

The diodes with Ni electrodes showed a different relation between the current density at RT for the samples with and without the $Al_2O_3$ interlayer as plotted in Fig. 7. A two-order-of-magnitude increase in the current density was observed. $\phi_B$ was 0.95 eV for the sample without the interlayer and 0.82 eV for the sample with the interlayer. $\phi_B$ was decreased by 130 meV upon the insertion of the $Al_2O_3$ interlayer. The ideality factors were 1.07 and 1.09 for the samples with and without the interlayer, respectively.

When the Pt electrodes were used, the current density at RT was almost the same for the samples with and without the $Al_2O_3$ interlayer as plotted in Fig. 8. $\phi_B$ was 0.98 eV for the sample without the interlayer and 0.96 eV for the sample with the interlayer. The ideality factors were 1.35 and 1.15 for the samples with and without the interlayer, respectively.

Although Al and Ti electrodes were also investigated, they led to ohmic behavior. This result is in agreement with a previous report [22]. In this work, only the electrodes with rectifying behavior were investigated because the determination of the SBH at an ohmic contact is complicated.

**Figure 6** *J–V* characteristics of the Au-electrode samples at RT.

Figure 9 summarizes $\phi_B$ vs the metal work function, $\phi_M$, for all the samples. The work functions of the metals were obtained from Ref. [22]. It can be seen that the Fermi level pinning is more severe for the samples with the $Al_2O_3$ interlayer. The solid lines are the fitting lines. The *S* factor is defined as [23]

$$S = \frac{d\phi_B}{d\phi_M}, \tag{3}$$

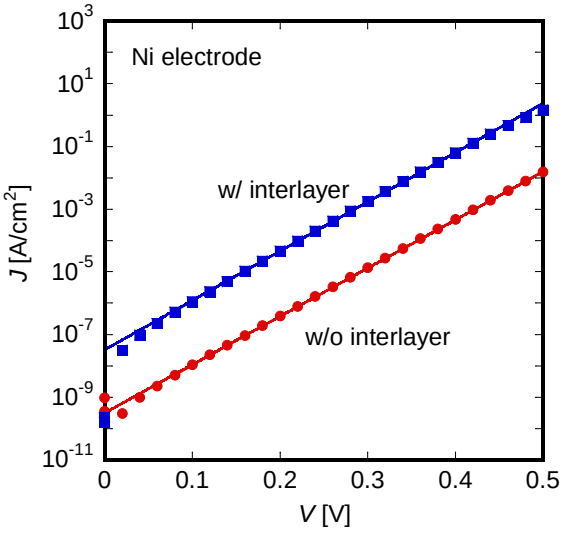


**Figure 7** *J–V* characteristics of the Ni-electrode samples at RT.

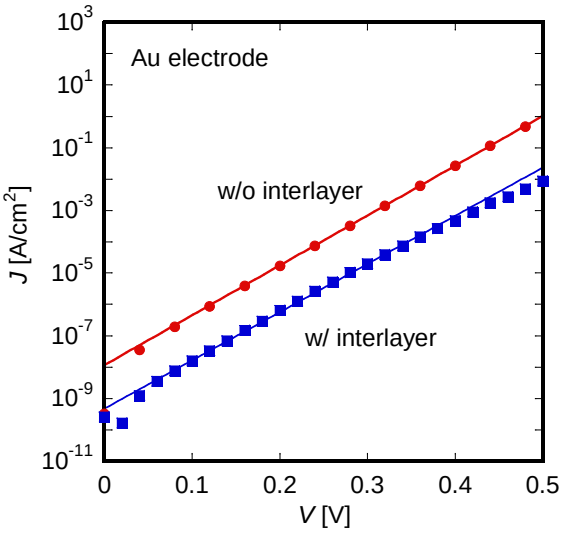


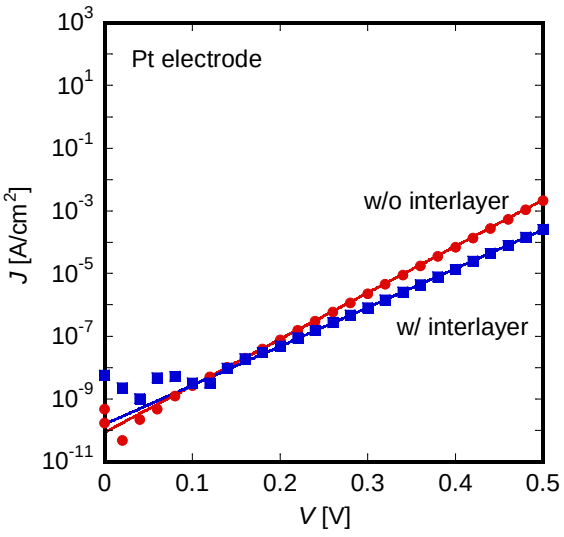

**Figure 8** *J–V* characteristics of the Pt-electrode samples at RT.

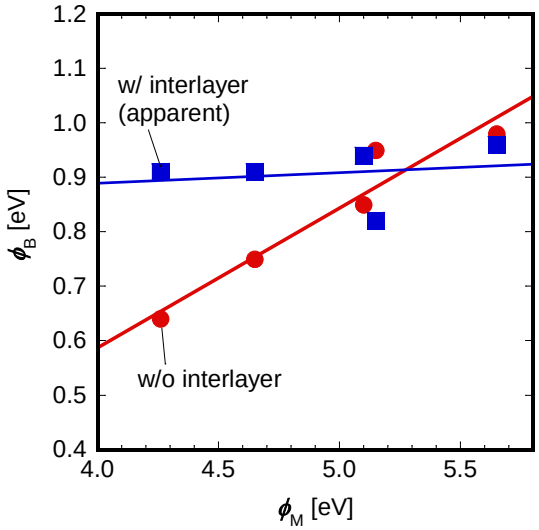


**Figure 9** Measured SBHs plotted against metal work function. Solid lines are fitting lines.

which is 0.26 for the samples without the $Al_2O_3$ interlayer but 0.019 for the samples with the interlayer. The inverse relation for the current density observed for the Ni-electrode samples, as shown in Fig. 7, is considered to be within the experimental error. Although blocking or attenuation of the metal wave function by using an ultrathin insulator was expected to lead to depinning, the pinning became stronger upon the insertion of the interlayer. The MIGS model cannot explain this result.

Enhanced metal-work-function dependences of the SBH have been reported for metal/$TiO_2$/Si [3], metal/NiO/Si [5], and metal/SiN/Ge [6] contacts. Although a 1-nm-thick ALD $Al_2O_3$ interlayer minimized the contact resistance at the Al/GaAs interface, the SBH was almost independent of the metal work function [8]. In addition, no discernible metal-work-function dependence of the SBH was observed for Al/ALD $Al_2O_3$(2 nm)/InGaAs structures [9, 10]. In particular, in Ref. [9], Fermi level pinning was discussed for a metal/InGaAs interface with an ALD $Al_2O_3$ interlayer. Although a reduction of the contact resistance has been reported for Ni/ALD $AlO_x$(1-2 nm)/n-Si and Ni/ALD $AlO_x$(1-2 nm)/p-Si contacts, depinning should have resulted in a reduction in the contact resistance of one of them but not both [4]. Therefore, the $Al_2O_3$ interlayer did not achieve depinning in terms of its real meaning.

In an MIS structure with a thick $Al_2O_3$ layer, the interface state density at the $Al_2O_3$/GaN interface formed by ALD is low even without annealing [21]. Nevertheless, strong pinning was observed for the present samples with the ultrathin $Al_2O_3$ interlayer. On the basis of the disorder-induced gap state (DIGS) model [23, 24], the Fermi level pinning is caused by interface disorder, which generates the

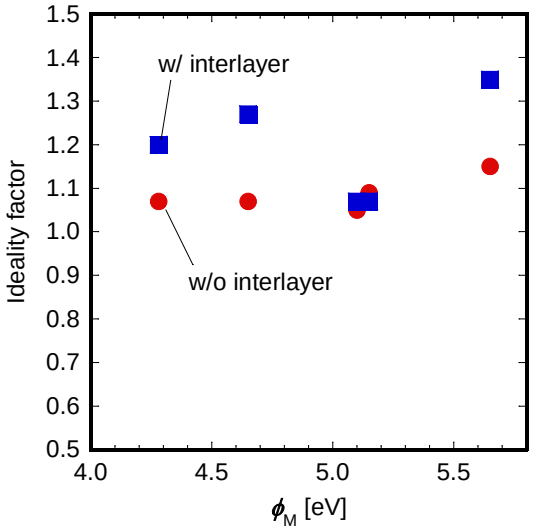


**Figure 10** Measured ideality factors plotted against metal work function.

interface states. According to an X-ray photoelectron spectroscopy study reported elsewhere [25], the chemical bonds at the topmost surface of the ALD $Al_2O_3$ layer exhibit a different component from those existing inside the bulk $Al_2O_3$. The $Al_2O_3$ surface may be chemically instable. The instability or reactivity of the $Al_2O_3$ surface may have caused the disorder at the metal/$Al_2O_3$ interface, which may have affected the $Al_2O_3$/GaN interface when the insulator layer was very thin. As shown in Fig. 10, slight increases in the ideality factors were observed for the samples with the interlayer, which may have resulted from the increase in interface disorder or interface states.

For the samples with the interlayer, an estimation of the interface state density from the ideality factor was reported in Ref. [26], in which the following equation was used:

$$n = 1 + \frac{(d/\varepsilon_i)\{(\varepsilon_s/W) + qD_{sb}\}}{1 + (dqD_{sa}/\varepsilon_i)}. \quad (4)$$

Here $d$ and $\varepsilon_i$ are the thickness and dielectric constant of the interlayer, respectively, $\varepsilon_s$ is the dielectric constant of the semiconductor, $W$ is the depletion layer width, $D_{sa}$ is the density of states in equilibrium with the metal, and $D_{sb}$

is the density of states in equilibrium with the semiconductor. For example, the relation between $D_{sa}$ and $D_{sb}$ required to achieve $n$ = 1.35 (the largest value in Fig. 10) is plotted in Fig. 11 for two different $W$ values, which indicates that physically possible parameters can explain the observed large ideality factor.

Strictly speaking, for the samples without the interlayer, fitting based on the TE model may contain a tiny error because the mean free path is much shorter than the depletion

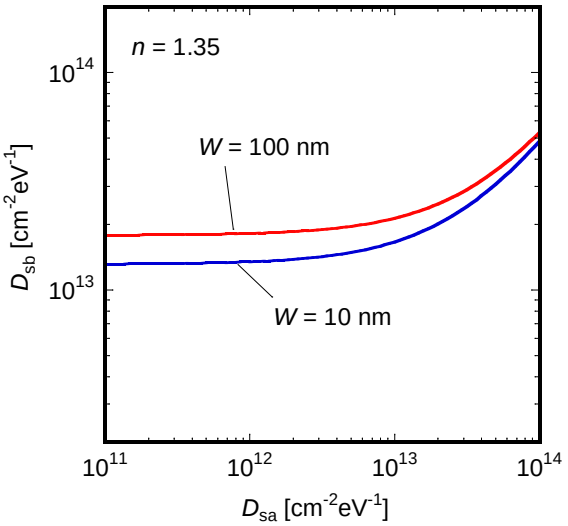


**Figure 11** Plot of $D_{sb}$ vs $D_{sa}$ required to achieve $n$ = 1.35 in Eq. (4) for $W$ = 100 nm and 10 nm.

layer width in GaN [19], which becomes significant at elevated temperatures [20]. However, according to Ref. [20], "the current is limited by the TE process in a GaN Schottky barrier diode at room temperature," although the thermionic emission-diffusion (TED) model should be applied at elevated temperatures. Furthermore, the present $\phi_B$ is 0.95 eV for the Ni/GaN interface without the interlayer, which is very close to the value obtained by the rigorous simulation (0.98 eV) [19]. Therefore, the TE model can be safely used to evaluate $\phi_B$ at RT for the samples without the interlayer.

**4 Summary** The effect of the insertion of an ultrathin $Al_2O_3$ layer at metal/GaN interfaces has been examined. The insertion of the $Al_2O_3$ interlayer caused the apparent SBH to change by as much as 270 meV depending on the metal work function. However, the apparent SBH for the samples with the interlayer was almost constant and independent of the metal electrode, although the samples without an interlayer exhibited a moderate dependence of the SBH on the metal work function. Although blocking or attenuation of the metal wave function by using an ultrathin insulator was expected to lead to depinning, the pinning became stronger upon the insertion of the interlayer.

**Acknowledgements** The authors are grateful to Prof. T. Hashizume and Prof. E. Sano for fruitful discussions. The authors also appreciate Dr. T. Narita, Toyota Central Research Labs., for providing the GaN epitaxial wafers.

## References

[1] S. M. Sze and K. K. Ng, Physics of Semiconductor Devices, 3rd edition (John Wiley & Sons, Inc., Hoboken, 2007), chap. 3 and chap. 8.
[2] D. Connelly, C. Faulkner, P. A. Clifton, and D. E. Grupp, Appl. Phys. Lett. **88**, 012105 (2006).
[3] A. Agrawal, J. Lin, M. Barth, R. White, B. Zheng, S. Chopra, S. Gupta, K. Wang, J. Gelatos, S. E. Mohney, and S. Datta, Appl. Phys. Lett. **104**, 112101 (2014).
[4] P. J. King, E. Arac, S. Ganti, K. S. K. Kwa, N. Ponon, and A. G. O'Neill, Appl. Phys. Lett. **105**, 052101 (2014).
[5] R. Islam, G. Shine, and K.C. Saraswat, Appl. Phys. Lett. **105**, 052103 (2014).
[6] M. Kobayashi, A. Kinoshita, K. Saraswat, H.-S. P. Wang, and Y. Nishi, J. Appl. Phys. **105**, 023702 (2009).
[7] J.-Y. J. Lin, A. M. Roy, A. Nainani, Y. Sun, and K. C. Saraswat, Appl. Phys. Lett. **98**, 092113 (2011).
[8] J. Hu, K. C. Saraswat, and H.-S. P. Wang, J. Appl. Phys. **107**, 063712 (2010).
[9] R. Wang, M. Xu, P.D. Ye, and R. Huang, J. Vac. Sci. Technol. B **29**, 041206 (2011).
[10] L. Chauhan, S. Gupta, P. Jaiswal, N. Bhat, S.A. Shivashankar, and G. Hughes, Thin Solid Films **589**, 264 (2015).
[11] R. Adari, D. Banerjee, S. Ganguly, and D. Saha, Thin Solid Films **550**, 564 (2014).
[12] V. Heine, Phys. Rev. **138**, A1689 (1965).
[13] J. Tersoff, Phys. Rev. Lett. **52**, 465 (1984).
[14] H. Amano, M. Kito, K. Hiramatsu, and I. Akasaki, Jpn. J. Appl. Phys. **28**, L2112 (1989).
[15] S. Nakamura, T. Mukai and M. Senoh: Appl. Phys. Lett. **64**, 1687 (1994).
[16] Y. Yue, Z. Hu, J. Guo, B. Sensale-Rodriguez, G. Li, R. Wang, F. Faria, B. Song, X. Gao, S. Guo, T. Kosel, G. Sinder, P. Fay, D. Jena, and H. Xing, Jpn. J. Appl. Phys. **52**, 08JN4 (2013).
[17] T. Oka, T. Ina, Y. Ueno, and J. Nishii, Appl. Phys. Express **8**, 054101 (2015).
[18] J. Suda, K. Yamaji, Y. Hayashi, T. Kimoto, K. Shimoyama, H. Namita, and S. Nagao, Appl. Phys. Express **3**, 101003 (2010).
[19] K. Mochizuki, A. Terano, T. Ishigaki, T. Tsuchiya, T. Mishima, and N. Kaneda, J. Mod. Math. Front. **3**, 29 (2014).
[20] T. Maeda, M. Okada, M. Ueno, Y. Yamamoto, T. Kimoto, M. Horita, and J. Suda, Appl. Phys. Express **10**, 051002 (2017).
[21] S. Kaneki, J. Ohira, S. Toiya, Z. Yatabe, J. T. Asubar, and T. Hashizume, Appl. Phys. Lett. **109**, 162104 (2016).
[22] A. C. Schmitz, A. T. Oing, M. Asif Khan, Q. Chen, J. W. Yang, and I. Adesia, J. Electron. Mater. **27**, 255 (1998).
[23] H. Hasegawa, Y. Koyama, and T. Hashizume, Jpn. J. Appl. Phys. **38**, 2634 (1999).
[24] H. Hasegawa and H. Ohno, J. Nac. Sci. & Technol. B **4**, 1130 (1986).
[25] M. Akazawa and T. Nakano, Appl. Phys. Lett. **101**, 122110 (2012).
[26] H. C. Card and E. H. Rhoderick, J. Phys. **D4**, 1589 (1971).